IEEE Access
Multidisciplinary | Rapid Review | Open Access Journal

Received March 3, 2019, accepted March 18, 2019, date of publication March 28, 2019, date of current version April 11, 2019.

Digital Object Identifier 10.1109/ACCESS.2019.2907970

Synchronization Procedure in 5G NR Systems

AYMEN OMRI[1], (Member, IEEE), MOHAMMED SHAQFEH[1], (Member, IEEE), ABDELMOHSEN ALI[2], (Member, IEEE), AND HUSSEIN ALNUWEIRI[1], (Senior Member, IEEE)

[1]Department of Electrical and Computer Engineering, Texas A&M University at Qatar, Doha, Qatar
[2]Department of Electrical and Computer Engineering, Concordia University, Montreal, QC H3G 1M8, Canada

Corresponding author: Aymen Omri (aymen.omri@qatar.tamu.edu)

This work was supported by the Qatar National Research Fund (a member of Qatar Foundation) through the National Priorities Research Program (NPRP) under Grant 8-1545-2-657. The statements made herein are solely the responsibility of the authors.

ABSTRACT Similar to all mobile communication networks, synchronization in the time–frequency domain is a fundamental step that allows a fifth-generation (5G) new radio (NR) user equipment (UE) to properly receive and transmit its data. Due to the wide range of frequencies that are defined for the 5G NR systems, the corresponding synchronization procedure becomes critical and presents many challenges, especially for the applications that would need accurate oscillators to reduce the large values of the frequency offset. In this paper, we present and detail the 5G NR physical layer. Then, we describe the required synchronization procedure for 5G NR. And finally, we present the main challenges and issues within the 5G NR synchronization.

INDEX TERMS 5G NR systems, beam management, physical layer, frequency offset, time offset, synchronization procedure.

I. INTRODUCTION

Fifth generation (5G) new radio (NR), the mobile communication standard presented by the 3rd generation partnership project (3GPP) as the 3GPP Release 15 [1]–[3], presents a major improvement of the long term evolution-advance (LTE-A) standard, where the main focus is on enhanced mobile broadband, ultra-reliable and low latency communications, and massive machine-type communications. To achieve these goals, 3GPP has introduced a unified network architecture, with a new physical layer design that supports very high carrier frequencies (mmWaves), large frequency bandwidths, and new techniques such as massive multiple-input and multiple-output (MIMO), and beamforming [1]–[3].

Those major modifications increase the synchronization procedure challenges.

In fact, the very high defined carrier frequencies result in large values of frequency and time offsets, which need an accurate and expensive oscillator to align a transmitter and a receiver for interference free communications. The sources of interference are mainly related to the imperfections of orthogonal frequency-division multiplexing (OFDM) systems, which suffer from the time and frequency offsets that result in inter-carrier interference (ICI), and inter-symbol interference (ISI) [4]–[7]. The time offset is due to the transmission delay, where the transmitted signal reaches the receiver delayed in time [8], [9]. In this case, the receiver does not know when the transmitter sent a new burst. Usually, the normalized timing offset is considered, which is equal to the number of samples between the transmitted signal and the received signal [4], [6]. If the normalized timing offset is larger than the cyclic prefix (CP) length, then a misalignment of the fast Fourier transform (FFT) window can be observed, which results in ISI and ICI. Otherwise, only a phase offset can be observed [4], [6]. The estimation and correction of the time offset should be done in the pre-FFT synchronization stage, by using specific synchronization algorithms. In the literature, the auto-correlation and cross-correlation algorithms are well known and used in wireless communication systems [10], [11]. In the first algorithm, the received signal is correlated with a delayed version of the same signal. However, in the second algorithm, the received signal is correlated with a stored pattern known to the receiver to estimate the time offset [4], [6]. Beside the time offset, the errors in the transmitter and the receiver oscillators result in frequency offset, which is a linear phase over the time domain samples and it causes ICI over the subcarriers [10], [12], [13]. In contrast to the time offset, this phase offset increases in time as it is directly proportional to the discrete time index. The frequency offset in OFDM

The associate editor coordinating the review of this manuscript and approving it for publication was Walid Al-Hussaibi.

is usually normalized to the sub-carrier spacing as the ratio between the frequency error and the sub-carrier spacing. In addition, a mismatch between the sampling frequency at both transmitter and receiver presents another source for the time offset.

In addition, the 3GPP has introduced a new high-dimensional phased arrays based mechanism to establish highly directional transmission links between the next generation node base station (gNB) and the user equipments (UEs). This mechanism requires fine alignment of the transmitter and the receiver beams, achieved through a set of operations known as beam management. The beam management needs complex algorithms and high level processing at gNBs and UEs to perform a variety of control tasks, including initial access, and beam tracking [14], which increase the synchronization procedure challenges.

In the reminder of this paper, the 5G NR physical layer is presented and detailed in Section II. In Section III, the required synchronization procedure and steps for 5G NR are described. Then, the main challenges and issues within the 5G NR synchronization are investigated in Section IV. Finally, conclusions are drown in Section V.

II. OVERVIEW OF 5G NR PHYSICAL LAYER

In this section, we present an overview of the 5G NR physical layer. The 3GPP references that detail all the specifications of the 5G NR as well as the used versions in this paper are presented in Table 1.

TABLE 1. 3GPP 5G NR specifications [15].

Specification	Version	Title
38.201	V15.0.0 (2017-12)	General Description
38.202	V15.4.0 (2018-12)	Service Provided by the Physical Layer
38.211	V15.4.0 (2018-12)	Physical Channels and Modulation
38.212	V15.4.0 (2018-12)	Multiplexing and Channel Coding
38.213	V15.4.0 (2018-12)	Physical Layer Procedures for Control
38.214	V15.4.0 (2018-12)	Physical Layer Procedures for Data
38.215	V15.4.0 (2018-12)	Physical Layer Measurements

Based on these 3GPP specifications, we present and detail in the following the 5G NR physical channels and signals as well as the frame structure.

A. PHYSICAL CHANNELS AND SIGNALS

The different 5G NR physical channels and signals are presented in Fig. 1 [1]. To figure out the differences between the 5G NR and the LTE in terms of physical channels and signals, we present in Table 2, a comparison between the two standards for each physical channel and each physical signal, where SHCCH denotes the shared and control channels.

B. 5G NR FRAME STRUCTURE

Based on the 3GPP specifications in [1], the 5G NR frame structure is described in this subsection. The 5G NR frame structure consists of $N_{subframe}^{frame} = 10$ subframes each of 1 ms. Different than LTE frame, each 5G NR subframe has

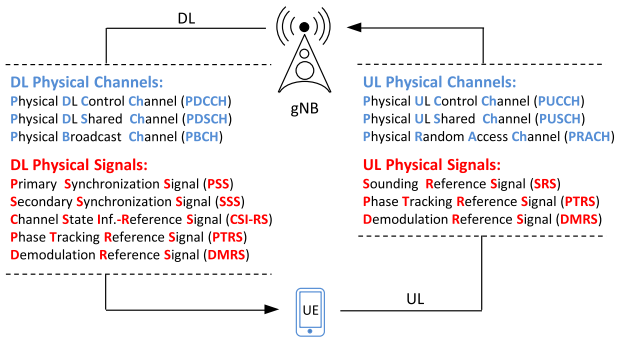

FIGURE 1. 5G NR physical channels and signals.

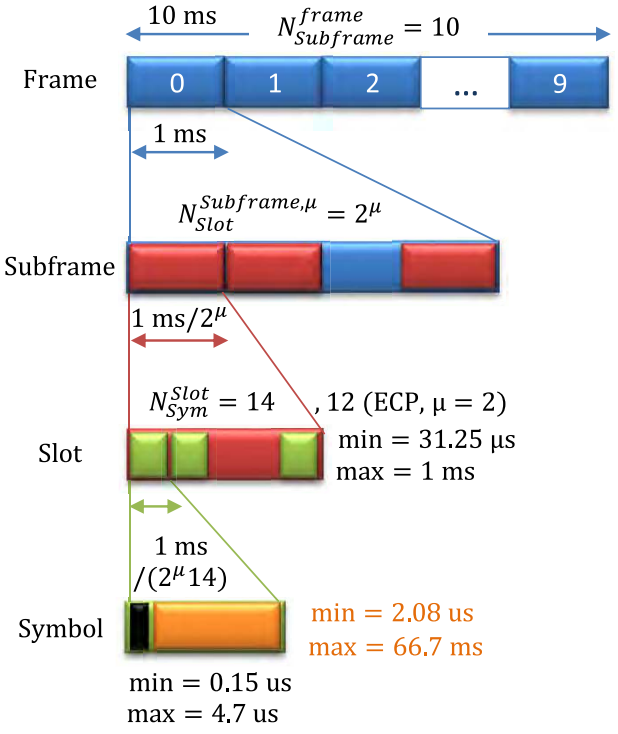

FIGURE 2. 5G NR frame structure.

flexible number of slots, which depends on the used numerology (μ). As presented in Fig. 2, this number is given by $N_{Slot}^{Subframe,\mu} = 2^{\mu}$. Consequently, the time slot period is equal to 1 ms / 2^{μ}. And, for each slot, there are 14/12 OFDM symbols, denoted by N_{Sym}^{Slot}, for normal/extended cyclic prefix, CP. Based on that, each symbol duration is equal to 1 ms / [$2^{\mu} \times 14$] (1 ms / [$2^{\mu} \times 12$]) for normal/extended CP. This is the frame structure in time domain.

In frequency domain, and similar to LTE standard, a resource block (RB) is defined as 12 consecutive subcarriers. Let Δf denotes the subcarrier spacing. In 5G NR, Δf is flexible and depends on the used numerology, e.g., $\Delta f = 2^{\mu} \times 15$ [kHz].

In the following, we focus on the time-frequency structure of the 5G synchronization block (SS/PBCH), which is denoted by SSB. Overall description on the

TABLE 2. Channels and signals: NR vs. LTE [1], [2].

		LTE	NR
Bandwidth	SHCCH	From 1.4 to 20 MHz	From 4.32 to 400 MHz
Type of Coding	PDSCH	Turbo	LDPC
	PDCCH	TBCC	Polar
	PBCH	TBCC	Polar
	PUSCH	Turbo	LDPC
	PUCCH	Block	Polar/Block
Type of SS sequences	PSS	Zadoff-Chu (ZC)	m-sequence
	SSS	m-sequence	Gold sequence
	DMRS	Gold sequence (DL), ZC (UL)	Gold sequence
	CSI-RS	Gold sequence	Gold sequence
	PTRS	NA	Gold sequence
	SRS	Gold sequence or ZC	Gold sequence
	PRACH	ZC	m-sequence
	PUCCH	ZC (e.g., ACK/NACK)	ZC (e.g., ACK/NACK)
Type of Modulation	PDSCH	Up to 256 QAM	Up to 256 QAM
	PDCCH	QPSK	QPSK
	PBCH	QPSK	QPSK
	PUSCH	Up to 64 QAM	$\pi/2$-BPSK and Up to 256 QAM
	PUCCH	BPSK / QPSK	BPSK / QPSK

TABLE 3. Resource allocation for SS/PBCH block [1, Tab. 7.4.3.1-1], l and k are relative to the beginning of the SS/PBCH block.

Channel or Signal	OFDM Sym. # (l)	Subcarrier. # (k)
PSS	0	56, 57, ..., 182
SSS	2	56, 57, ..., 182
Set to 0	0	0, ..., 55, and 183, ..., 239
	2	48, ..., 55, and 183, ..., 191
PBCH	1, 3	0, 1, ..., 239
	2	0, ..., 47, and 192, ..., 239
DMRS for PBCH	1, 3	$0+v$, $4+v$, ..., $236+v$
	2	$0+v$, $4+v$, ..., $44+v$, and $192+v$, $196+v$, ..., $236+v$

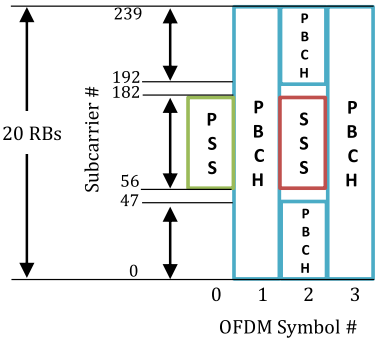

FIGURE 3. Resource allocation for SSB.

resource allocation for SSB is described in Table 3 [1, Tab. 7.4.3.1-1], where $v = N_{\text{ID}}^{\text{Cell}} \bmod 4$, and $N_{\text{ID}}^{\text{Cell}}$ is the corresponding physical cell ID.

Based on Table 3, the summary of the SSB specification are as follows:

- SS (PSS and SSS) and PBCH in NR is transmitted in the same 4 symbol block.
- SSB consists of 240 contiguous subcarriers (20 RBs).
- The subcarriers are numbered in increasing order from 0 to 239 within the SSB.

Table 3 can be represented in resource grid as shown in Fig. 3. This SSB structure is general and defined for all the numerology in 5G NR. However, for a half frame, the number and first symbol indexes for candidate SSBs are different and determined according to the corresponding subcarrier spacing as follows [3]:

- **Case A -** 15 **kHz Subcarrier Spacing**: The first symbols of the candidate SSBs have indexes of $\{2, 8\} + 14 \times n$. For carrier frequencies smaller than or equal to 3 GHz, $n = 0,$ and 1. For carrier frequencies larger than 3 GHz and smaller than or equal to 6 GHz, $n = 0, 1, 2,$ and 3.
- **Case B -** 30 **kHz subcarrier spacing**: the first symbols of the candidate SSBs have indexes $\{4, 8, 16, 20\}+28 \times n$. For carrier frequencies smaller than or equal to 3 GHz, $n = 0$. For carrier frequencies larger than 3 GHz and smaller than or equal to 6 GHz, $n = 0,$ and 1.
- **Case C -** 60 **kHz subcarrier spacing**: the first symbols of the candidate SSBs have indexes $\{2, 8\} + 14 \times n$. For carrier frequencies smaller than or equal to 3 GHz, $n = 0,$ and 1. For carrier frequencies larger than 3 GHz and smaller than or equal to 6 GHz, $n = 0, 1, 2,$ and 3.
- **Case D -** 120 **kHz subcarrier spacing**: the first symbols of the candidate SSBs have indexes $\{4, 8, 16, 20\} + 28 \times n$. For carrier frequencies larger than 6 GHz, $n = 0, 1, 2, 3, 5, 6, 7, 8, 10, 11, 12, 13, 15, 16, 17,$ and 18.
- **Case E -** 240 **kHz subcarrier spacing**: the first symbols of the candidate SSBs have indexes $\{8, 12, 16, 20, 32, 36, 40, 44\} + 56 \times n$. For carrier frequencies larger than 6 GHz, $n = 0, 1, 2, 3, 5, 6, 7,$ and 8.

C. SYNCHRONIZATION SIGNALS

Similar to 4G networks, the synchronization signals PSS and SSS are used in 5G NR systems to help the UEs to get radio

frame boundary and to detect the cell identity (ID). In 5G NR systems, each radio cell is identified by a cell ID from 1008 IDs that are arranged into 336 different groups. Each group is identified by the cell ID group, $N_{ID}^{(1)} \in \{0, \ldots, 335\}$, and consists of three different sectors, which are specified by the cell ID sector, $N_{ID}^{(2)} \in \{0, 1, 2\}$. The UE can detect the value of $N_{ID}^{(2)}$ from the PSS, and the value of $N_{ID}^{(1)}$ from the SSS. Based on that, the UE computes the serving cell ID as follows: $N_{ID}^{cell} = 3\,N_{ID}^{(1)} + N_{ID}^{(2)}$. The 5G NR cell ID concept is the same as in 4G networks. However, the number and the generation of the corresponding synchronization signal sequences are different. In the following, we present these differences, and the details of the 5G NR signal generations.

1) PSS

In 4G networks, each PSS consists of one of three 62-symbols Zadoff-Chu sequences and is mapped to the central 72 subcarriers with a guard band of 10 subcarriers. For FDD frame, PSS is allocated on symbol # 6 (last symbol) of slot # 0 (subframe 0) and slot # 10 (subframe 5) of each radio frame. And, for TDD frame, PSS is allocated on symbol # 2 of slot # 2 (subframe 1) and slot # 12 (subframe 6) of each radio frame.

Similar to 4G networks, the 5G-NR PSS is a physical layer specific signal and helps UEs to get radio frame boundary, and to detect the cell ID sector, e.g., $N_{ID}^{(2)}$. However, the 5G NR PSS consists of one of three 127-symbols m-sequences and is allocated on the first symbol of each SSB, and on 127 subcarriers. The 3 possible m-sequences for the PSS are defined as follows [1]

$$d_{PSS}(n) = 1 - 2\,x(m), \tag{1}$$

where,

$$m = \left[n + 43\,N_{ID}^{(2)}\right] \bmod 127, \quad 0 \le n < 127, \tag{2}$$

$$x(i+7) = [x(i+4) + x(i)] \bmod 2, \tag{3}$$

and,

$$[x(6)\,x(5)\,x(4)\,x(3)\,x(2)\,x(1)\,x(0)] = [1\;1\;1\;0\;1\;1\;0]. \tag{4}$$

2) SSS

In 4G networks, each SSS consists of one of 168 62-symbols m-sequences. Similar to PSS, the SSS is mapped to the central 72 subcarriers with a guard band of 10 subcarriers. For FDD frame, SSS is allocated on symbol # 5 of slot # 0 (subframe 0) and slot # 10 (subframe 5) of each radio frame. And, for TDD frame, SSS is allocated on symbol # 6 (last symbol) of slot # 1 (subframe 0) and slot # 11 (subframe 5) of each radio frame.

Similar to 4G networks, the 5G-NR SSS is used to detect the cell ID group, e.g., $N_{ID}^{(1)}$. However, the 5G NR PSS consists of one of 336 127-symbols gold sequences and is allocated on the third symbol of each SSB, and on 127 subcarriers. The 336 possible gold sequences for the SSS are defined as follows [1]

$$d_{SSS}(n) = [1 - 2x_0\,([n + m_0] \bmod 127)] \times [1 - 2x_1\,([n + m_1] \bmod 127)], \tag{5}$$

where,

$$m_0 = 15\left\lfloor \frac{N_{ID}^{(1)}}{112} \right\rfloor + 5\,N_{ID}^{(2)}, \tag{6}$$

$$m_1 = N_{ID}^{(1)} \bmod 112, \quad 0 \le n < 127, \tag{7}$$

$$x_0(i+7) = [x_0(i+4) + x_0(i)] \bmod 2, \tag{8}$$

$$x_1(i+7) = [x_1(i+4) + x_1(i)] \bmod 2, \tag{9}$$

$$[x_0(6)\,x_0(5)\,x_0(4)\,x_0(3)\,x_0(2)\,x_0(1)\,x_0(0)] = [0\;0\;0\;0\;0\;0\;1], \tag{10}$$

and,

$$[x_1(6)\,x_1(5)\,x_1(4)\,x_1(3)\,x_1(2)\,x_1(1)\,x_1(0)] = [0\;0\;0\;0\;0\;0\;1], \tag{11}$$

III. SYNCHRONIZATION PROCEDURE IN 5G NR SYSTEMS

Due to the wide range of the new defined frequencies in 5G NR systems, the corresponding synchronization procedure becomes more critical and presents many challenges. Recently, the synchronization procedure in 5G NR systems is presented in [3]. In this section, the main steps of the 5G NR synchronization procedure are detailed first. Then, numerical results are presented to evaluate this procedure.

A. MAIN STEPS OF 5G NR SYNCHRONIZATION

The 5G NR synchronization procedure is based on the beam management operations, including (i) initial access for idle users, which allows a mobile UE to establish a physical link connection with a gNB, and (ii) beam tracking, for connected users, which enable handover, beam adaptation, and radio link failure recovery procedures. The beam management is based on four different operations; (i) Beam sweeping, (ii) Beam measurement, (iii) Beam determination, and (iv) Beam reporting. Based on theses four operations, we present in Fig. 4, the general 5G NR synchronization procedure, which can be summarized as follows:

By using a beam sweeping, the gNB periodically transmits SS burst that carries multiple SSBs, with periodicity $T_{SS} = \{5,\ 10,\ 20,\ 40,\ 80,\ \text{or}\ 160\}$ ms [14]. As shown in Fig. 5, each SSB is transmitted via a specific beam with pre-specified interval and direction. The SSBs in a half frame are indexed in an ascending order in time from 0 to $L - 1$.

For initial access case (idle mode), the UE should start by the cell search procedure. By using the PSS, SSS, and specific synchronization algorithms, the UE can estimate and correct the frequency and time offsets. In the next subsection, we present and details some well know and used synchronization algorithms in the literature.

After decoding the PSS, the UE can detect the cell ID sector ($N_{ID}^{(2)}$). Then, by using the detected $N_{ID}^{(2)}$, the UE can decode

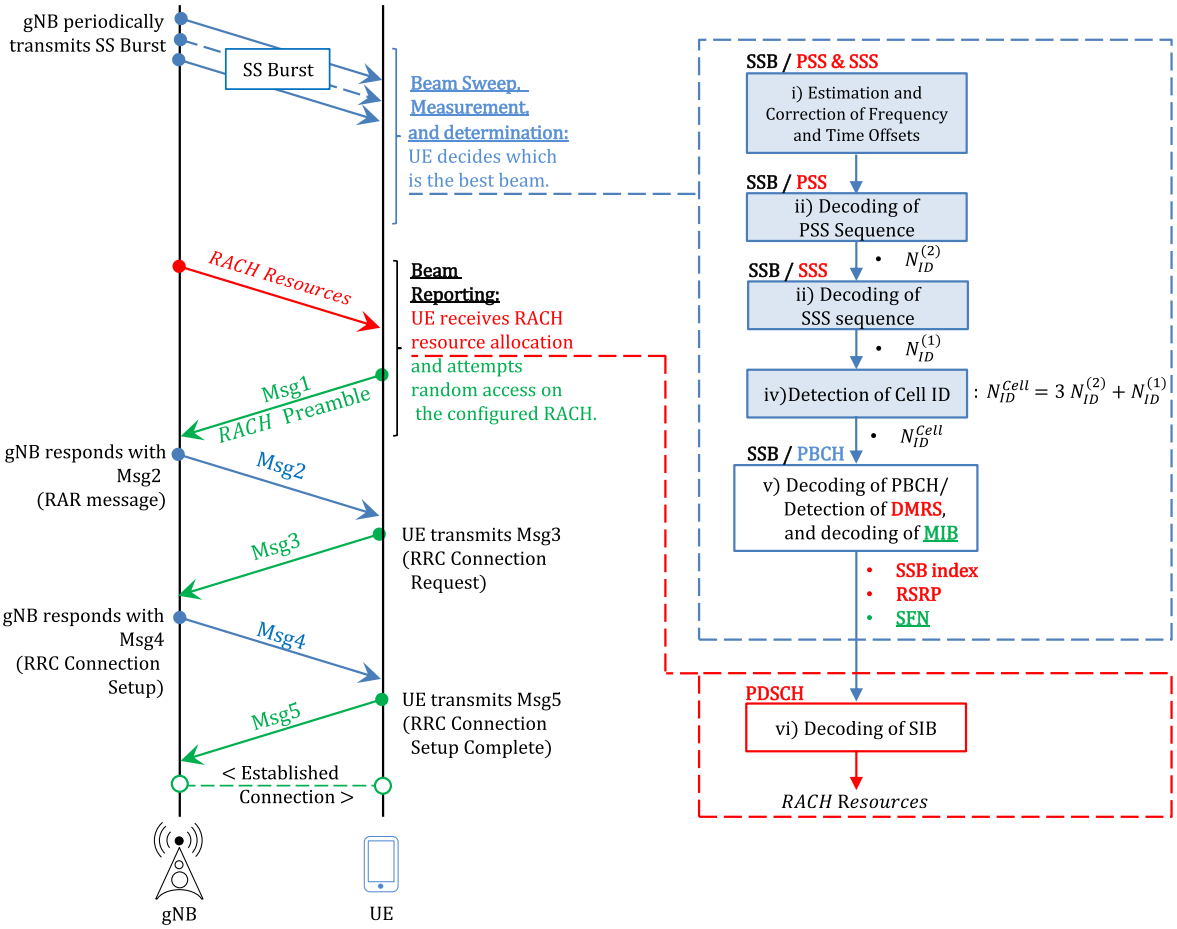

FIGURE 4. 5G NR synchronization procedure.

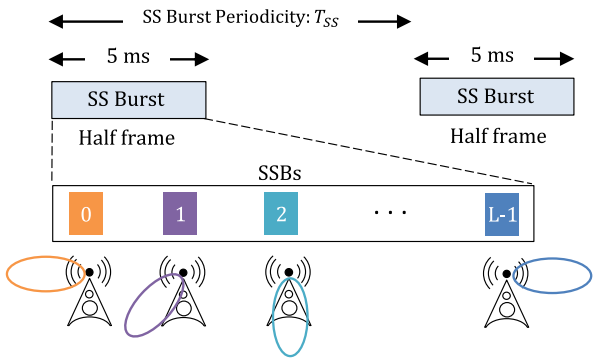

FIGURE 5. SS burst transmission.

the SSS and detect the cell ID group $N_{ID}^{(1)}$, and hence it can compute the serving cell ID as follows: $N_{ID}^{cell} = 3N_{ID}^{(1)} + N_{ID}^{(2)}$.

After detecting the cell ID, the UE should identify the candidate SSB within the SS burst (set of L SSBs). As we have detailed in Subsection II. B, for each subcarrier spacing, there is a set of candidate SSBs with different first symbol indexes per a half-frame. Each SSB is corresponding to a specific beam. So, to detect the serving beam index, the UE should identify the corresponding SSB index (0, 1, 2, .. or $L-1$). Based on the received PBCH, the UE shall determine the 2 least significant bits (LSBs), for $L = 4$, or the 3 LSBs, for $L > 4$, of the candidate SSB index per half frame from a one-to-one mapping with an index of the DMRS sequence transmitted in the PBCH. The rest of the SSB index is carried by the PBCH data.

For example, let us consider the case of 15 kHz subcarrier, a carrier frequency less than 3 GHz, and $L = 4$. Based on that, the SBBs are allocated at symbol indexes 2, 8, 16, and 22. Each of them has a unique SSB index, i_{SSB}, (2 bits in this case) and is corresponding to unique sample timing, which refers to the sample accurate timing, e.g., the sample corresponds to the first sample, of a given symbol, in a given slot per a frame. Therefore, the UE can detect the i_{SSB} from decoding the corresponding PBCH, where the corresponding DMRS is a function of i_{SSB}. For example, if the UE successfully decodes the PBCH with a DMRS carries $i_{SSB} = 0$, then the corresponding SSB is mapped to symbol 2 of the half-frame, and then the UE can detect the sample timing within the 5 ms.

After that, the UE has to know which 5 ms is this in a radio frame (the first 5 ms or the second 5 ms). This extra bit is provided by the master information block (MIB), and also by

the DMRS in case of $L = 4$. So after decoding the PBCH, the UE knows the sample timing within the full frame.

In addition to the sample timing, the UE should detect the system frame number (SFN). The SFN is divided into two parts (i) 4 LSBs that are used within the channel encoding of the MIB message itself, and (2) 6 most significant bit (MSBs) that are part of the MIB data. During the MIB decode, there will be blind decode trials since UE does not know the 4 LSBs of the MIB that are used during the channel encoding. So, it will try different combinations while decoding the MIB, each corresponds to a unique 4 LSBs. One of them should get into success, and then the UE will know the 4 LSBs of the SFN. Hence, once the MIB is decoded successfully, the corresponding SFN will be known in full.

The decoded DMRS (associated with the PBCH) can be used to measure the reference signal received power (RSRP) of the candidate SSB, which can be used for the beam measurement, with the other measurements of the RSRP, and the reference signal reported quality (RSRQ) given by SSS.

Based on the beam measurement, the beam determination can be done and the UE can decide which is the best beam.

During the beam reporting, and based on the necessary parameters that are including in the MIB, the UE can decode the system information block (SIB) that is transmitted by the gNB over PDSCH and includes the RACH resources. Based on that, the UE can transmit Message 1 (RACH preamble) on the configured RACH resources via the selected beam.

After receiving Message 1, the gNB responds with Message 2 (random access response (RAR)). Then, the UE transmits Message 3 (RRC connection request), and the gNB sends Message 4 (RRC connection setup) to the UE. Finally, the UE sends to the gNB Message 5 (RRC connection setup complete).

Once random access procedure is completed, dedicated connection is established between UE and gNB with dedicated connection ID.

These procedures are used to update the optimal transmitter and receiver beam pair over time.

For beam tracking case (connected mode), the beam management operations use CSI-RS (in DL) and SRS (in UL) to transfer the beam/CSI report and the DL control information (DCI) between the gNB and the UE, and to update the connection via the strongest selected beam.

For initial access case (idle mode), as we detailed before, the beam management operations use PSS, SSS and PBCH DMRS, where the cell search procedure is required to detect the cell ID. The cell search procedure is a crucial step in the 5G NR synchronization as it needs accurate time and frequency offsets detection and correction. In the following we focus on the details of this procedure.

To access to the network or during a handover operation, the UE has to acquire correct timing and frequency synchronization to recover the cell ID of the serving gNB. This first operation is known as initial cell-search, which can use different algorithms of estimation and correction of frequency and time offsets. These synchronization algorithms are neither provided nor presented in the 3GPP specifications. In the literature, the cross-correlation and auto-correlation methods are well known and used in wireless communication systems [10], [11]. In the following, we details these two correlation based synchronization algorithms that can be used in 5G NR Networks.

1) CROSS-CORRELATION SYNCHRONIZATION ALGORITHM USING PSS

In this cross-correlation process, the received signal is correlated with the PSS stored pattern known to the receiver. The cross-correlation based algorithm can be summarized as follows: Let $r(n)$ be the perfect received signal in the discrete time domain, which is expressed as follows:

$$r(n) = s(n) \otimes h(n) + w(n), \tag{12}$$

where, $s(n)$ is the transmitted signal, $h(n)$ is the channel impulse response (CIR), $w(n)$ is the noise term, and $\otimes$ is the linear convolution operator. In the presence of carrier frequency offset (CFO), the received signal expression becomes

$$r_\epsilon(n) = \Big[s(n) \otimes h(n) + w(n)\Big] \exp\Big(\frac{j2\pi n}{N_{\text{FFT}}}\epsilon\Big), \tag{13}$$

where, ϵ is the normalized frequency offset to the sub-carrier spacing, which can be separated into integer frequency offset (IFO: ϵ_I), and fractional frequency offset (FFO: ϵ_F). Let $\hat{\theta}$ denotes the estimated timing synchronization position of PSS, and $\hat{i} \in \{0, 1, 2\}$ denotes the estimate of cell ID sector. By using the time-domain received signal, a joint estimation of $\hat{\theta}$ and $\hat{i}$ can be done based on the following criterion [10], [11]

$$(\hat{\theta}, \hat{i}) = \arg\max_{\theta, i}(C(\theta, i)), \tag{14}$$

where, $C(\theta, i)$ is the cross-correlation, which is expressed as [11]

$$C(\theta, i) = \frac{\Big|\sum_{k=0}^{N_{\text{FFT}}-1} r(\theta + k)p_i^*(k)\Big|}{\sum_{k=0}^{N_{\text{FFT}}-1} |r(\theta + k)|^2}. \tag{15}$$

Here, $r(\theta + k)$ presents the delayed received signal, $p_i(k)$ denotes the PSS sequence time-domain waveform of cell ID sector i, and N_{FFT} is the FFT number without CP. Based on that, the FFO estimation can be evaluated as follows [11]

$$\hat{\epsilon}_F = \frac{1}{\pi}\angle\Bigg(\Bigg[\sum_{k=0}^{N_{\text{FFT}}/2-1} r(\hat{\theta} + k)p_{\hat{i}}^*(k)\Bigg]^* \times \Bigg[\sum_{k=N_{\text{FFT}}/2}^{N_{\text{FFT}}-1} r(\hat{\theta} + k)p_{\hat{i}}^*(k)\Bigg]\Bigg), \tag{16}$$

where, $\angle(.)$ and $[.]^*$ are the argument and complex conjugate operators, respectively.

The PSS based cross-correlation synchronization algorithm is efficient for small values of CFO, as $\hat{\epsilon}_F$ in equation (16) presents the estimate FFO only.

2) AUTO-CORRELATION SYNCHRONIZATION ALGORITHM USING CP

In this auto-correlation method, a part of the received signal is correlated with the corresponding CP part. The auto-correlation based algorithm can be summarized as follows: Let $\gamma(\theta)$ and $\alpha(\theta)$ denote the correlation and energy terms, which are expressed as

$$\gamma(\theta) = \sum_{k=\theta}^{\theta+L-1} r(k)r^*(k+N_{FFT}), \tag{17}$$

and,

$$\alpha(\theta) = \sum_{k=\theta}^{\theta+L-1} |r(k)|^2 + |r(k+N_{FFT})|^2, \tag{18}$$

respectively, where L is the CP length. Based on that, the maximum likelihood (ML) can be used to estimate θ and ϵ as follows [11]

$$\hat{\theta} = \max_{\theta} (2|\gamma(\theta)| - \rho\angle(\theta)), \tag{19}$$

and,

$$\hat{\epsilon} = -\frac{1}{2\pi}\angle(\gamma(\hat{\theta})), \tag{20}$$

where, ρ is the magnitude of the correlation coefficient between $r(k)$ and $r(k+N)$, which is expressed as

$$\rho = \frac{\sigma_S^2}{\sigma_S^2 + \sigma_N^2}, \tag{21}$$

with σ_S^2 and σ_N^2 are the signal and the noise powers, respectively.

This method's accuracy can be improved by averaging the estimates of time and frequency offsets over several OFDM symbols. In a large CFO scenario, i.e., $\epsilon > 1$, the FFO can be estimated by using the auto-correlation algorithm, and the IFO can be recovered in the frequency domain, by evaluating the shift of the received PSS. This method is insensitive to IFO and can offer an accurate estimation of FFO before the estimation of IFO, which is not the case for the cross-correlation method. However, the auto-correlation method cannot provide the cell ID.

As presented in Fig. 4, the estimation and correction of time-frequency offset is a crucial task in the overall 5G NR synchronization procedure. In the following sub-section, we present numerical results to investigate the 5G NR synchronization procedure.

B. NUMERICAL RESULTS AND INTERPRETATIONS

The conducted simulation parameters are provided in Table 4 and represent typical values representative of numerology 3 of 5G NR network.

The used 5G NR channel model is the tapped delay line (TDL)-A, where the corresponding channel parameters are presented in Table 5.

The conducted numerical results is based on our developed 5G NR simulator, which uses the corresponding 3GPP specifications to evaluate the average BER for different time-frequency synchronization scenarios.

TABLE 4. Simulation parameters.

Parameter	Value
Numerology: μ	3
Carrier Frequency	20 GHz
Sub-Carrier Frequency Spacing	120 kHz
Modulation	QPSK
Slot Duration	0.125 ms
Symbol Duration	8.92 μs
Useful Symbol Duration	8.32 μs
CP Duration	0.60 μs
N_{RB}	275
Bandwidth	396 MHz
FFT Size: N_{FFT}	4096
Cell ID	0
PSS Sequence	m-Sequence
E_b/N_o	0 to 20 dB

TABLE 5. Power-delay profile of TDL-A channel [16].

Normalized Delay	Power in [dB]
0.0000	-13.4
0.3819	0
0.4025	-2.2
0.5868	-4
0.4610	-6
0.5375	-8.2
0.6708	-9.9
0.5750	-10.5
0.7618	-7.5
1.5375	-15.9
1.8978	-6.6
2.2242	-16.7
2.1718	-12.4
2.4942	-15.2
2.5119	-10.8
3.0582	-11.3
4.0810	-12.7
4.4579	-16.2
4.5695	-18.3
4.7966	-18.9
5.0066	-16.6
5.3043	-19.9
9.6586	-29.7

Fig. 6 presents a performance comparison between cross-correlation and auto-correlation algorithms in terms of time offset estimation error. It is clear here that both algorithms offer good performances in terms of time offset estimation error, with a slightly advantage of the auto-correlation method for $\theta = 5$. These results confirm that both methods are efficient and able to offer a good estimation of time-frequency offset.

The impacts of time and frequency offsets on BER, with different values of ϵ, $\theta = 4$, and $\hat{\theta} = 4$ are presented in Fig. 7. As shown in this figure, for small values of ϵ, the two methods are able to estimate and correct the frequency offset to offer an acceptable BER. By increasing the values of ϵ, the auto-correlation method outperforms the cross-correlation method as it can offer a low CFO estimation error. However, for high CFO values, e.g., $\epsilon > 0.5$, both method suffer from

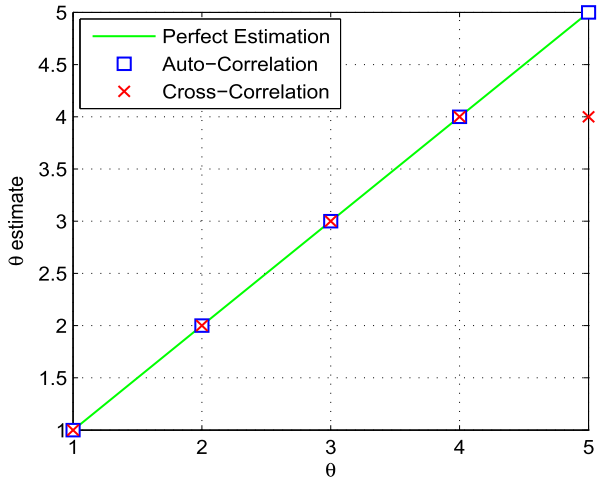

FIGURE 6. Comparison of the time-offset estimation for cross-correlation and auto-correlation algorithms.

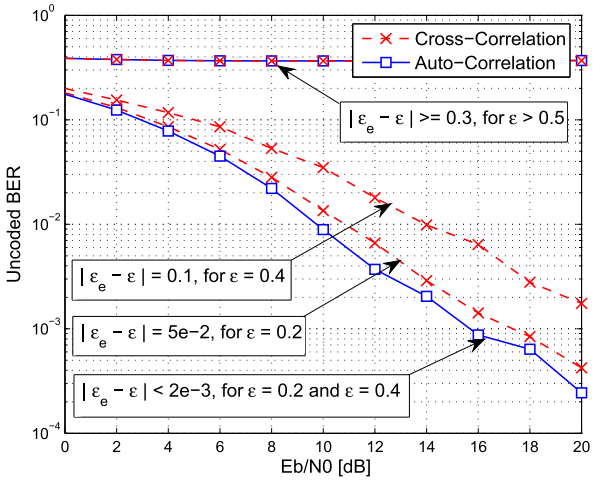

FIGURE 7. Impact of time and frequency offsets on BER, with different values of ϵ, $\theta = 4$ and $\hat{\theta} = 4$.

the high estimation error, which results in significant BER performance degradation.

In Fig. 8, we present the required accuracy (maximum allowed error) of a given oscillator that can be used in 5G NR to offer a maximum CFO equal to 0.2 and 0.4. This figure shows that the oscillator accuracy is decreasing with the increased values of the carrier frequency (F_C). This is because, for a fixed value of ϵ, F_C and the oscillator accuracy are inversely proportional; $\alpha = \frac{\epsilon \Delta f}{2 F_C}$. In addition, it is clear that the CFO increases with the increased values of the maximum allowed error of the oscillator, which is expected.

As shown in the simulation results, to offer an acceptable BER, the synchronization methods are able to manage only a specific range of CFO, e.g., $\epsilon < 0.4$. And to offer such values of CFO, an accurate oscillator is needed, where its accuracy is increasing with the increased values of the used carrier frequency, which presents a crucial issue for the 5G NR networks.

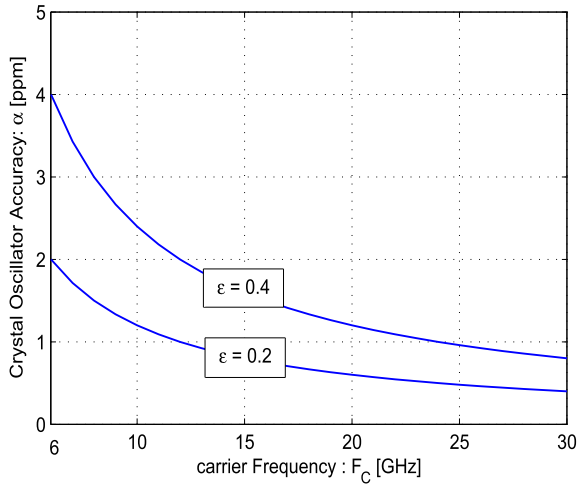

FIGURE 8. Trade-off between the crystal oscillator accuracy and the carrier frequency; $\alpha = \frac{\epsilon \Delta f}{2 F_C}$, for numerology $\mu = 3$.

Based on that, we present in the following sub-section, the main synchronization challenges in 5G NR systems.

IV. SYNCHRONIZATION CHALLENGES IN 5G NR SYSTEMS

The main challenge in 5G NR systems is the time-frequency synchronization in the presence of the wide range of the new defined frequencies. The new defined frequency band increases the imperfections of the used OFDM systems, which results in serious interference problems. To overcome this problems, new efficient synchronization procedure should be proposed, and a more accurate and expensive oscillator must be used. In fact, the frequency error is mainly related to the accuracy of the used oscillator, and the environment factors (mainly temperature) may deviate the used carrier frequencies. The frequency deviation is measured in parts per million (ppm), which is a value that represents the part of a whole number in units of $1/1000000$, i.e., one ppm is equal to $1/1000000$ of the whole:

$$1\text{ppm} = 1 \times 10^{-6} = 0.0001\%. \tag{22}$$

In wireless communication, the ppm indicates how much the used oscillator's frequency may deviate from the nominal value. For example, in LTE, a 10 ppm crystal oscillator is used for the frequencies range of 3GHs and below. It means, that for a given LTE equipment that is using a carrier frequency of 3 GHz, its frequency error is equal to $+/-$ 10 ppm $\times$ 3 GHz$=$ 30 kHz. Consequently, the real carrier frequency will be between (3 GHz-30 kHz) and (3 GHz+30 kHz), which presents the accuracy of the used oscillator. In LTE, this range is acceptable for frequency tolerance, where the corresponding frequency offset can be estimated and corrected during the synchronization procedure between the eNBs and the UEs. However, for 5G NR, a very wide range of frequencies is defined, which needs a very accurate oscillator, note that the oscillator's cost is inversely proportional to its ppm.

In addition, the used beamforming technique is based on precise alignment of the transmitter and the receiver beams, which needs complex algorithms and high level processing at gNBs and UEs. These algorithms and processing may increase the latency of establishing a link, and have important implications on control layer procedures, such as initial access, handover, and beam tracking.

In this context, many challenges for the 5G NR should be addressed:

- The current 10 ppm crystal oscillator that is used in LTE presents a high frequency offset, e.g., 60 kHz for 6 GHz. Based on that a more expensive oscillator should be used to offer less ppm, and hence less frequency offset.
- What is the maximum acceptable frequency error in 5G NR?
- How would the current commercial oscillators behave in the 5G NR?
- What is the expected accuracy for the current commercial oscillators?, and is it possible to offer an acceptable frequency error for the very wide range of the new frequencies?
- During the signaling procedure, are the gNBs and the users able to estimate and correct the frequency offset of the current commercial oscillators?
- Are the gNBs and the UEs able to use the proposed beamforming technique to establish a precise alignment of the transmitter and the receiver beams, especially for communication scenarios with mobility?

V. CONCLUSION

In this paper, we have described and investigated the synchronization procedure in 5G NR systems. First, we have detailed the 5G NR physical layer. Then, we have described the required synchronization procedure, and different synchronization algorithms for 5G NR. Based on that, numerical results are conducted and investigated to evaluate the synchronization procedure, and to present the main challenges, and issues within the 5G NR synchronization. As expected, the main challenge for the 5G NR systems is the time-frequency synchronization in the presence of the wide range of the new defined frequencies, and the performance limitation of the current commercial crystal oscillator.

REFERENCES

[1] *NR; Physical Channels and Modulation Release 15*, document TS 38.211, V.15.4.0, 3GPP, 2018.
[2] *NR; Multiplexing Channel Coding Release 15*, document TS 38.212, V.15.4.0, 3GPP, 2018.
[3] *NR; Physical Layer Procedures for Control Release 15*, document TS 38.213, V.15.4.0, 3GPP, 2018.
[4] M. A. Alvarez and U. Spagnolini, "Distributed time and carrier frequency synchronization for dense wireless networks," *IEEE Trans. Signal Inf. Process. Netw*, vol. 4, no. 4, pp. 683–696, Dec. 2018.
[5] H. Abdzadeh-Ziabari, W.-P. Zhu, and M. N. S. Swamy, "Joint maximum likelihood timing, frequency offset, and doubly selective channel estimation for OFDM systems," *IEEE Trans. Veh. Technol.*, vol. 67, no. 3, pp. 2787–2791, Mar. 2018.
[6] K. Shamaei and M. Sabbaghian, "Analytical performance evaluation of SC-FDMA systems in the presence of frequency and time offset," *IEEE Trans. Wireless Commun.*, vol. 14, no. 11, pp. 6230–6239, Nov. 2015.
[7] D. Li, Y. Li, H. Zhang, L. J. Cimini, and Y. Fang, "Integer frequency offset estimation for OFDM systems with residual timing offset over frequency selective fading channels," *IEEE Trans. Veh. Technol.*, vol. 61, no. 6, pp. 2848–2853, Jul. 2012.
[8] V.-T.-D. Huynh, N. Noels, and H. Steendam, "Effect of offset mismatch in time-interleaved ADC circuits on OFDM-BER performance," *IEEE Trans. Circuits Syst. I, Reg. Papers*, vol. 64, no. 8, pp. 2195–2206, Aug. 2017.
[9] A. M. Hamza and J. W. Mark, "Closed-form expressions for the BER/SER of OFDM systems with an integer time offset," *IEEE Trans. Commun.*, vol. 63, no. 11, pp. 4461–4473, Nov. 2015.
[10] R. Zeng, H. Huang, L. Yang, and Z. Zhang, "Joint estimation of frequency offset and Doppler shift in high mobility environments based on orthogonal angle domain subspace projection," *IEEE Trans. Veh. Technol.*, vol. 67, no. 3, pp. 2254–2266, Mar. 2018.
[11] S. Huang, Y. Su, Y. He, and S. Tang, "Joint time and frequency offset estimation in LTE downlink," in *Proc. 7th Int. Conf. Commun. Netw. China*, Aug. 2012, pp. 394–398.
[12] O. H. Salim, A. A. Nasir, H. Mehrpouyan, and W. Xiang, "Multi-relay communications in the presence of phase noise and carrier frequency offsets," *IEEE Trans. Commun.*, vol. 65, no. 1, pp. 79–94, Jan. 2017.
[13] C. Chen, Y. Chen, Y. Han, H.-Q. Lai, and K. J. R. Liu, "High resolution carrier frequency offset estimation in time-reversal wideband communications," *IEEE Trans. Commun.*, vol. 66, no. 5, pp. 2191–2205, May 2018.
[14] M. Giordani *et al.*, "A tutorial on beam management for 3GPP NR at mmWave frequencies," *IEEE Commun. Surveys Tuts.*, vol. 21, no. 1, pp. 173–196, Sep. 2018.
[15] 3GPP. *The 3rd Generation Partnership Project*. Accessed: Mar. 17, 2019. [Online]. Available: http://www.3gpp.org/
[16] *Study on Channel Model for Frequency Spectrum Above 6 GHz*, document TR 138.900, V.14.2.0, Jun. 2017.

AYMEN OMRI received the degree in telecommunication engineering from The Academy of Aviation (EABA), Tunisia, in 2007, and the M.Res. and Ph.D. degrees in telecommunications from the Engineering National School of Tunis (ENIT)/Tunis El Manar University, in 2009 and 2012, respectively.

From 2012 to 2017, he was a Postdoctoral Researcher with the Electrical Engineering (EE) Department, Qatar University. He is currently a Postdoctoral Researcher with the Department of Electrical and Computer Engineering, Texas A&M University at Qatar. His research interests include modeling, design, and performance analysis of wireless communication systems. His current specific research interests include device-to-device communications, UAV-based networks, and the fifth-generation (5G) wireless communication networks.

MOHAMMED SHAQFEH received the B.Sc. degree in electrical engineering (communications stream) from United Arab Emirates University, in 2003, the M.Sc. degree in communications technology from Ulm University, Germany, in 2005, and the Ph.D. degree from The University of Edinburgh, Edinburgh, U.K., in 2009. In 2009, he joined the Department of Electrical and Computer Engineering, Texas A&M University at Qatar, where he is currently an Associate Research Scientist. His research interests include wireless communication networks, information theory, and smart transportation systems.

ABDELMOHSEN ALI was born in Giza, Egypt, in 1982. He received the B.Sc. and M.A.Sc. degrees in electronics and communication engineering from Cairo University, Giza, in 2004 and 2008, respectively, and the Ph.D. degree in electrical and computer engineering from Concordia University, Montreal, QC, Canada, in 2016. From 2008 to 2012, he was with Wasiela, where he was involved in digital communications modem design including DVB-C/T2, and LTE. He is currently with Riot Micro as a Senior Lead for the IoT physical-layer solutions. He also serves as an affiliated Assistant Professor with Concordia University. His research interests include cognitive radio networks, multi-user communications, communication signal processing, VLSI architectures for communication systems, machine-to-machine communications, the Internet of Things, and 5G. He has received many awards, including the Best Paper Award of the WCNC 2016 and the Canadian Governor General's Academic Gold Medal 2017.

HUSSEIN ALNUWEIRI (S'81–M'83–SM'17) received the Ph.D. degree in electrical and computer engineering from the University of Southern California, Los Angeles, in 1989. From 1991 to 2007, he was a Professor with the Department of Electrical and Computer Engineering, The University of British Columbia. From 1996 to 1998, he represented The University of British Columbia, Vancouver, BC, Canada, at the ATM Forum. From 2000 to 2006, he served as a Canadian Delegate to the ISO/IEC JTC1/SC29 Standards Committee (MPEG-4 Multimedia Delivery), where he worked within the MPEG4 standardization JTC1-SC29WG11 Group to develop the first client–server MPEG4 video streaming reference software. He has a long record of industrial collaborations with several major companies worldwide. He is currently a Professor with the Department of Electrical and Computer Engineering, Texas A&M University at Qatar, Doha, Qatar. He is also an inventor and holds four U.S. patents. He has authored or coauthored more than 200 refereed journal and conference papers in various areas of computer and communications research. In particular, his research interests include the mobile Internet technologies, cyber security and cyber systems, mobile cloud computing, wireless communications, routing and information dissemination algorithms in mobile networking, and quality-of-service provisioning and resource allocation in wireless networks.